TECHNICAL MEMORANDUMS

NATIONAL ADVISORY COMMITTEE FOR AERONAUTICS

No. 1039

PRESSURE DISTRIBUTION IN NONUNIFORM TWO-DIMENSIONAL FLOW

By M. Schwabe

Ingenieur-Archiv, Vol. VI, No. 1, February 1935

Washington
January 1943

NATIONAL ADVISORY COMMITTEE FOR AERONAUTICS

TECHNICAL MEMORANDUM NO. 1039

PRESSURE DISTRIBUTION IN NONUNIFORM TWO-DIMENSIONAL FLOW*

By M. Schwabe

SUMMARY

The two-dimensional flow past a circular cylinder is made visible on the surface of water by scattered particles and recorded under long exposure by a moving picture camera. The velocity of flow is deduced from the path lengths of the particles, the radius of curvature of the paths is defined, the pressure along a streamline is determined according to Bernoulli's general formula ($p = p_o - \frac{1}{2}\rho w^2 - \rho \partial\Phi/\partial t$), and transverse to the streamlines according to the centrifugal force formula ($p = p_o + \rho \int v^2/r \, ds'$). The pressure distribution formulas for different stages of development of the vortex pair and for one state of the vortex street is indicated, the pressure field determined, the pressure drop behind the cylinder analyzed and the variation of the pressure drag coefficient with respect to time demonstrated. It reaches a value about twice as high as in the steady state. The asymmetrical pressure distribution on the cylinder is demonstrated for one stage of development of the vortex street and the force transverse to the flow direction defined; it amounts to more than 40 percent of the drag in this instance.

In the theoretical treatment the customary potential flow is superposed by a source-sink flow, the potential of which is secured by series development, from which the velocity components are deduced. In the pressure formula $p_o = \frac{1}{2}\rho w^2 + p + \rho \partial\Phi/\partial t$ the time variable $f(t)/a$ and its derivation are solved from the recorded motion of the free stagnation point.

A comparison of theory and experiment indicates good agreement in the streamline pattern. The approximation of the theoretical to the experimental pressure distribution on the zero streamline for an early state of development of

---

*"Über Druckermittlung in der nichtstationären ebenen Strömung." Ingenieur-Archiv, vol. VI, no. 1, February 1935, pp. 34-50.

the vortex pair is also satisfactory. Subsequent calculation indicates pronounced departures from the test data. The theoretical pressure field is compared with the experimental, the theoretical pressure curve on the line of symmetry behind the free stagnation point and the pressure drop in it dependent on the time is obtained in satisfactory approximation with the test data.

INTRODUCTION

In an attempt to follow the time rate of change of the processes in turbulent flows by quantitative measurements the measurement of the pressure is often beset with insuperable difficulties for the reason that the speeds and hence the pressures to be measured are often very small. On the other hand, the measurement of very small pressures requires, at least, considerable time, so that the follow-up of periodically varying processes is as good as impossible.

In order to obviate these difficulties a method, suggested by Prof. Prandtl, has been developed by which the pressure distribution is simply determined from the photographic flow picture. This method is described and proved on a worked-out example. It was found that quantitatively very satisfactory results can be achieved.

EXPERIMENT

1. Principles.- Ahlborn's method of visualization of two-dimensional flow on the surface of fluids by sprinkling with fine particles affords, by appropriate choice of experimental details, an insight into the periodically rapidly changing processes.

By sprinkling the water surface in such a manner that the separate particles are far apart in comparison to their size and taking a long-exposure picture so that the path lines of the particles can be clearly distinguished on the picture, the time of exposure and the length of the dashes are a measure of the mean velocities of the particles during the exposure. From subsequent records, what happens further can be seen and the accelerations thus determined.

From the velocities and accelerations the pressure distribution past a streamline can be determined by means of the generalized Bernoulli equation to the extent that the effect due to friction may be disregarded. Then the pressure gradient perpendicular to the streamline can be ascertained from the curvature of the path lines of the particles.

2. Experimental setup.- A tank 3.4 meters long, 0.59 meter wide and 0.48 meter deep was available through which a resistance body - in this instance a circular cylinder - could be towed (fig. 1). The cylinder stood on the bottom of a U-shape beam which was attached to a carriage in such a way that its walls during towing passed close along the sides of the tank. In this way the region under observation could be left free from interfering stopping devices. The carriage itself ran over the top edges of the side walls of the tank on rails, one of which served as guide rail. Owing to the appearance of a boundary layer and vortices on the upright tank walls during the run, removable side walls were inserted, so that the upright beam walls ran in a narrow space between tank wall and inserted wall. In this manner the experimental field remained free from vortices of foreign origin. The effect of the vortices on the bottom plate of the beam is not traceable until at relatively great distance behind the body; at any rate it did not interfer with the present tests. The inserted protective walls reduced the effective area of the tank to 340 X 50 centimeters.

To the side of the tank and separate from it stood the drive mechanism, a heavy frame with a spindle of 3 centimeters lead, which was driven over a reduction gear from an electric motor and by means of an automatic disengaging clutch pushed another carriage forward which could be coupled with the model carriage. This second carriage, running in the same way on rails like the first, supported a vertical column with movable arms for the lamps used to illuminate the surface of the water. A telescopic arm between the lamps held the photographic apparatus. So when the two carriages were coupled together and with the spindle the camera recorded pictures of the motion processes in a reference system, relative to which the body was at rest and the fluid flowed past it.

3. Photographic procedure.- The photographs were taken with a special kind of motion-picture camera. The ratio of the time of nonexposure, that is, essentially the time necessary for transportation of the film, to the time

of exposure was reduced to approximately 1:10 by means of the insertion of a "maltese cross" into the drive (reference 1).

The data on the speed of travel of the cylinder and the exposure needed for the evaluation were first obtained from the records with a chronograph as described by Rubach (reference 2). Subsequently the records were transferred on the picture. At the border of the camera field a second hand watch was fastened on the carriage, and also a scale, past which pointers soldered at certain distances to a metal band stretched over the tank moved at the same height during the run. The time of exposure was read from the watch, the length covered by the indicators on the scale, divided by the exposure, gave the running speed.

The end of the body sticking out of the water was covered with black velvet above which two stretched wires formed a system of axes. A further wire was stretched close to and in the center over the water surface, parallel to the guide rail. The body was disposed so that one of the crossed wires was parallel with the wire above the water and vertically under it. The moving picture camera with the objective lens, was arranged vertically over these two wires. The long wire thus halved the field of the camera and appeared on the pictures as line of symmetry of the body and vortex pair.

Inasmuch as the dashes on the photographs had to be plainly visible and easily measurable, the use of lycopodium spores was abandoned because of their small size in favor of screened aluminum particles which were scattered over the water just close enough to produce as many separate dashes as possible on the photographs without, however, causing the dashes to overlap.

The water was colored with the water soluble "dark red for dark room light" Mark highest, Agfa. This plotted out all details on the bottom and sides of the tank, leaving only the reflection of the light on the surface in the form of a fine veil on the negative (about 3 grams color per square meter of surface, independent of depth was added in solution). The time of exposure of the individual film pictures was chosen with respect to the running speed and in such a manner that the longest path lengths traveled by the particles during exposure amounted to about 3 centimeters. Agfa positive film was used.

4. Evaluation.- The next problem involved the measurement of the velocities, that is, the velocities maintained on the individual film pictures as path lengths of the separate particles per exposure of the particular picture. For this purpose the films were enlarged at two-thirds natural size with a Leitz enlarger Filix on 13 × 18 Agfa Brovira paper. The method was briefly as follows: The body contour was plotted at natural size in a rectangular system of coordinates, within the contour a short scale with millimeter divisions, and so photographed that a natural length of 15 centimeters was reproduced at a length of 10 centimeters. The thus obtained negative was copied on contrast film and this positive then placed on the enlargement paper to be exposed. The enlarger was set so that in the projection of the motion-picture film negative the cross hairs coincided with the experimental body, and the longitudinal axis of the tank and the body contour coincided with the corresponding parts on the contrast film. In that way the scale of reproduction was secured. The enlargement of the motion-picture film and of the coordinate system, copied at the same time, afforded a comprehensive division of the flow region near the body and rendered the identification of individual, frequently recurring points during the evaluation very convenient.

Now, in order to plot velocities we pick out a certain state for evaluation and attempt to trace by means of the short path lines a streamline s (fig. 2) which is not affected by friction, that is, not located in direct proximity of the body. In point of fact, it is even profitable to get away from the body as far as the field of the camera allows, as will be shown later. On the circular cylinder the path lines distant 2R from the center transverse to flow direction can be accepted as identical with the streamlines, without perceptible error. Then the streamline drawn from some chosen point is now plotted straight in natural length on millimeter paper. Bernoulli's formula along a streamline is used to determine the pressure differences

$$p_1' - p_2' = \rho\left(\frac{\partial}{\partial t} \int_{p_1'}^{p_2'} \underline{v}\, d\, \underline{s} + \frac{v_2^2}{2} - \frac{v_1^2}{2} \right) \qquad (1)$$

where v is the velocity at the momentary point on the streamline in its direction; $1/2\, v_1^2$ and $1/2\, v_2^2$ are easily

found. The velocities are computed for a number of points on the streamline from the dash lengths of the photographic records, the one-half square values are computed and plotted; then the gaps between the test points are bridged by a curve which enables the particular value $1/2 v_n^2$ for any point P_n' of the streamline to be read off. The integral requires the determination of the time rate of change of v in a point of the streamline, or more exactly, the time rate of change of the component of v in direction of ds.

In consequence one picture is insufficient and the selected state is considered as mean value of the preceding and of the subsequent state, in which, generally, different velocities are found for a point fixed in space. The chosen streamline is sketched on transparent paper and then transferred to these two pictures, where, it is true, it is not streamline; but at the chosen distance from the body the deviation is so small as to introduce no perceptible error when the velocities are plotted as described and the minor angular variations of the path lines along the basic streamline onto which the two additional pictures were transferred are disregarded. So, when the velocities from these pictures are plotted it will be seen (fig. 3) that they increase behind the body and the area between the two curves is the difference of our integral $\int v\,ds$ over two exposure periods. The numerical value of this integral is obtained graphically, and then divided by $2B$, where B equals the time of exposure plus the time necessary for transportation of film; the velocity in the interval of the three observed pictures being assumed to increase linearly with the time.

The pressure differences transverse to the streamline are determined according to

$$p_2' - p_2 = \rho \int_{P'_2}^{P_2} \frac{v^2}{r}\, ds' \qquad (2)$$

r being the curvature radius of the path lines and s' a line intersecting the path lines in the direction of their curvature radii. The different lines s' are secured by moving outward from the body perpendicularly to the streamlines as far as the basic streamline. The starting points should be chosen so as to afford a suitable basis for plotting the pressure curve. Like the streamline, the vertical

lines are, drawn in natural length and recorded the same way as the velocities. The v^2 curve is easily obtained from the test points (figs. 4a and 4b).

To determine the curvature radii a number of circular arcs are plotted, the diameters inscribed, the whole photographed at two-thirds natural size and copied on contrast film. By sliding this arc scale over the picture we seek the circular arc that coincides with the chosen path lines or we interpolate by eye. The reciprocal values $1/r$ are recorded. The curve for v^2/r (figs. 4a and 4b) encloses with s' our $\int \frac{v^2}{r} \, ds'$; its value is also graphically ascertained.

The most appropriate starting point for the pressure calculation is the forward stagnation point P_1. Standardizing the pressure of undisturbed flow far from the body at $p_o = 0$, the pressure at the stagnation point is $p_1 = \frac{1}{2}\rho a^2$, a being the velocity at infinity and the carriage speed, respectively.

Then the pressures can be inscribed without difficulty. The pressure p'_1 at the intersection P'_1 of the vertical line s'_1 from the forward stagnation point P_1 with the streamline s is

$$p'_1 = p_1 + \rho \int_{P'_1}^{P'_1} \frac{v^2}{r} \, ds'$$

$\frac{v^2}{r}$ being negative in this instance, the integral value is to be deducted from the amount.

The pressure p'_1 is the starting point for the prediction of the pressure on the streamline. According to equation (1) the pressure p'_n at the point of intersection P'_n of line s'_n with streamline s is

$$p'_n = p'_1 + \rho \frac{v_1^2}{2} - \rho \left(\frac{\partial}{\partial t} \int_{P_1'}^{P_1} \underline{v} \, d\underline{s} + \frac{v_n^2}{2} \right)$$

Next we determine the pressures in the intersections of the vertical lines with the streamline in order to ascertain from these points with (2) the pressures at the cylinder circumference. The obtained values are divided by p_1 for dimensionless representation and plotted against φ as abscissa.

5. Evaluation results.- In this manner the pressure curves for different stages of development of the vortex pair are secured, as exemplified in figure 6, for a test with $a = 0.82$ centimeter per second. The individual stages, chosen at random, are illustrated in figures 5a to 5e. The accompanying dashed curve represents the pressure variation for the usual potential flow; d denotes the distance of the free stagnation point* from cylinder center referred to cylinder radius. It is seen that with advancing development of the vortex pair the pressure in the rear stagnation point drops quickly at the same time as the pressure minimum halfway between forward and rear stagnation point flattens out and shifts toward the forward stagnation point. The curves approach in their aspect the well-known experimental pressure curve for stationary flow, but, on account of the continuous variation of the flow and pressure conditions, it is scarcely to be expected that they actually will ever assume their shape. The carriage speed a used in the test for the comparison with the calculations, was 0.82 centimeter per second. The velocity head to be read on a manometer, is $h = \frac{a^2}{2g} = 0.000342$ centimeters of water column. This indicates the pressure in the forward stagnation point.

The selection of streamline s at the border of the camera field enables the prediction of the pressure for any chosen point on lines s' by extension of the integral of $\frac{v^2}{r}$ over s' only up to this point. The points of equal pressure are connected by curves. (See figs. 7a and 7b.) Here also the shift of the pressure minimum from $\pi/2$ toward π is plainly evident; for the rest, the representations can speak for themselves.

---

*The free stagnation point moves, on motion from rest, from the rear stagnation point of the cylinder; in it the zero streamline, which divides in the forward stagnation point and encloses cylinder together with vortex pair, closes again; d is chosen as characteristic for the particular state.

The determination of the pressures on the zero streamline needed for the comparison of the mathematical and experimental data is secured by extending the integral of $\frac{v^2}{r}$ over s' only from the basic streamline to the point of intersection of s' with the zero streamline.

The pressure distribution on the line of symmetry from the rear stagnation point for three earlier stages of development of the vortex pair was obtained also (figs. 5a to 5c) and plotted in figure 8 against r/R. (R = radius of cylinder, r = distance of point from center; hence $r/R = 1$ is the rear stagnation point). The points of the momentarily obtained pressure in the free stagnation point are joined together by a dashed curve. Between the rear stagnation point at the cylinder and the free stagnation point exists a pressure minimum; the pressure in the free stagnation point is higher than at the body, but the pressure maximum is higher yet and lies beyond the free stagnation point in the non-vortical flow. This leads to the following explanation which, of course, still requires a more accurate framing: The pressure rise on the rear side of the cylinder is sufficient not only to let the particles existing in the boundary layer and slowed down by the friction, come to rest before reaching the stagnation point but to actually repulse them. Herewith a pressure equalization is associated, that is, a pressure rise in the negative pressure zone and a pressure drop in the positive pressure zone. The pressure in the rear stagnation point which, after all, is within the boundary layer, may therefore well drop below the pressure outside of the boundary layer, so that particles from the stagnation point must move away from the cylinder against a pressure rise, which also lets them, before reaching the pressure maximum, come to rest – in the free stagnation point – and drives them back to the cylinder, where they then follow the other particles into the zone of the pressure minimum. The process of pressure equalization with respect to time is apparent from the three curves.

For the determination of the pressure drag W and its coefficient $c_w = \frac{W}{2 R \rho a^2/2}$, respectively, the curves of figure 6 are plotted, instead of against φ, against the distance y from the line of symmetry and then integrated.

The so obtained coefficients are shown in figure 9 plotted against the time in dimensionless presentation. We see that c_w increases slowly at first, but then very rapidly, and exceeds the value 2. What occurs further is without the scope of the present evaluation. In the present test with Reynolds number Re = 580 a pressure drag coefficient of about 1 would be expected for the steady state. We see that within a short time it increases to about double and does not drop within the range of the evaluations; this does not occur until the vortex pair separates from the cylinder. The high c_w during the first vortex formation – the cylinder is no longer subjected to accelerations – is probably due to the fact that the energy consumption for the enlargement of the vortices is very high.

At this point reference is made to experiments by F. S. Schmidt (reference 3) who made photographic records of the velocities of spheres falling in water and of ascending balloons. He established in the acceleration zone a speed maximum below the terminal velocity, followed by a minimum which coincides with the maximum of the drag coefficient. Schmidt also indicated an approximate representation for the maximum of the drag coefficient for the scope of his experiments. He correlated maximum and minimum velocity with the vortex formation. The minimum was reached at separation of the vortex ring (vortex pair, at cylinder).

The methods described here are not restricted to the vortex pair. Figure 11 shows the pressure distribution for a state of the vortex strut of figure 10. The pressure values are plotted against the cylinder circumference from the forward over the rear and back again to the forward stagnation point. The unsymmetry of the curve is plainly visible. The integration gives $c_w = 1.09$, the Reynolds number is Re = 735. The pressure forces on the cylinder transverse to the flow direction occurring by alternating vortex formation and evidenced in the asymmetry of the pressure curve, can be determined by plotting the pressures on the cylinder circumference against the diameter that lies in the flow direction, and follow it by integrating. Referred to the dynamic pressure like the pressure drag we find as coefficient $c_a = 0.447$. The pressure transverse to the flow direction therefore is in the present case more than 40 percent of the drag pressure. Figure 12 shows the pressure drag in magnitude and direction,

the transverse pressure and its resultant. The eccentric position of the point of application was secured graphically from polygon of forces and funicular polygon. The transverse force swings from one side to the other in correspondence with the vortex separation.

It should be remembered that the pressure distribution in a limited flow diverges, of course, from that in the unlimited flow. The pressure minimum is lower. In our case an approximation by Ermisch (reference 4) can be roughly accepted, that is, that the potential pressure curve due to the limiting walls reaches a minimum of -5.2 instead of -3.0 by unlimited flow; it is shown as dotted curve in figure 16 in support of the estimation of the effect of the walls on the recorded pressure distribution. More accurate predictions are not possible. In the subsequent calculations the wall effect is discounted.

THEORY

In order to represent the processes on a circular cylinder at incipient vortex formation, mathematically, the analytical expression for the customary potential flow must be extended in such a way that the zone, occupied by the growing vortex pair, is in some form replaced. Proceeding from a more empirical theorem suggested by Prof. Prandtl, the space, occupied by the growing vortex pair, is assumed to contain a type of source-sink flow. The results, of course, then restrict the comparison with the real flow to the space outside of the vortex zone, but become, as such, very informative. Thus two systems of flow, the common potential flow and the additional source-sink flow must be superposed.

1. Ideal flow.- The complex stream function of the ideal non-vortical flow past a circular cylinder (reference 5) is

$$F(z) = Ra\left(z + \frac{1}{z}\right) = Ra\cos\varphi\left(\frac{r}{R} + \frac{1}{r/R}\right) + iRa\sin\varphi\left(\frac{r}{R} - \frac{1}{r/R}\right) \qquad (1)$$

where a is the velocity of undisturbed flow, r the distance from center of cylinder, R the cylinder radius

and φ the angle measured from the rear stagnation point. The real constituent gives the potential

$$\Phi_1 = R\,a \cos\varphi\left(\frac{r}{R} + \frac{1}{r/R}\right) \tag{2}$$

and the imaginary constituent the stream function

$$\psi_1 = R\,a \sin\varphi\left(\frac{r}{R} - \frac{1}{r/R}\right) \tag{3}$$

The velocity w_1 at some point is decomposed in its radial v_{r_1} and tangential v_{φ_1} components.

$$v_{r_1} = \frac{\partial\Phi_1}{\partial r} = a \cos\varphi\left(1 - \frac{1}{(r/R)^2}\right) \tag{4}$$

and

$$v_{\varphi_1} = \frac{1}{r}\frac{\partial\psi_1}{\partial\varphi} = -\,a \sin\varphi\left(1 + \frac{1}{(r/R)^2}\right) \tag{5}$$

2. The additional source-sink flow.- In this replacement of the growing vortex pair by a source-sink flow a theorem of the chosen kind, unfortunately affords only an approximate representation of the very first beginnings. Figure 13 indicates the contour of the cylinder and the zone of the vortex pair enveloped by the zero streamline. The upper half of the sketch shows the form in which this zone can be filled by a source-sink flow. The travel of the point of separation from the rear toward the forward stagnation point is disregarded and a continuous distribution of sources and sinks at the cylinder circumference is assumed in such a manner that the yield from π to $\pi/2$ equals zero and from $\pi/2$ to 0 follows a law as indicated on the lower half of figure 13. To comply with the equation of continuity, if Q is the yield of the sources and sinks, it must

$$\int_0^{\pi/2} Q\,d\varphi = 0$$

Q is dependent of the position at the cylinder circumference, hence of φ and, because of the growth of the zone of the vortex pair, of the time t.

The potential, which is to be added to the ideal potential flow in order to obtain the outside flow at incipient separation, is secured by expansion in series. Thus the additional potential Φ_2, is written in the form

$$\Phi_2 = f(t) \Sigma c_n r^{-n} \cos n\varphi$$

This series satisfies Laplace's differential equation $\Delta\Phi = 0$ and disappears for large r. The coefficients c_n are defined by dictating the radial velocity of the additional flow on the cylinder circumference, that is, according to the viewpoints laid down for the source-sink distribution. For fixed r the series is a Fourier series. Standardizing the cylinder radius R at 1, the radial velocity of the additional source-sink flow at the cylinder circumference is

$$v_{r_2} = \left(\frac{\partial \Phi_2}{\partial r}\right)_{r=R} = f(t) \Sigma - n c_n \cos n\varphi$$

$$= f(t) F(\varphi)$$

and for any chosen r, which must be referred to cylinder radius R,

$$v_{r_2} = \frac{\partial \Phi_2}{\partial r} = f(t) \Sigma - n c_n \left(\frac{r}{R}\right)^{-n-1} \cos n\varphi$$

$$= f(t) \Sigma C_n \left(\frac{r}{R}\right)^{-n-1} \cos n\varphi$$

Let us stipulate that for $0 \leqq \varphi \leqq \frac{\pi}{2}$

$$F(\varphi) = -\tfrac{1}{2}(\cos 2\varphi + \cos 4\varphi) \qquad (6)$$

and for $\frac{\pi}{2} \leqq \varphi \leqq \pi$

$$F(\varphi) = 0$$

The expansion of $F(\varphi)$ in Fourier series, broken off with the term $\cos 9\varphi$, gives

$$F(\varphi) = -(0.085 \cos\varphi + 0.25 \cos 2\varphi + 0.327 \cos 3\varphi + 0.25 \cos 4\varphi + 0.101 \cos 5\varphi - 0.018 \cos 7\varphi + 0.006 \cos 9\varphi) \quad (7)$$

In less important cases such as the construction of the streamline pattern the approximation is fully sufficient when the series is stopped with $\cos 5\varphi$; but for the pressure distribution all the shown terms are necessary. The time dependent $f(t)$ must be determined by means of experiment.

3. The combined ideal and source-sink flow.- Now the question regarding the additional potential and concerning the total potential and the velocity components of the flow past the cylinder together with the vortex pair can be answered. The total potential is

$$\Phi = \Phi_1 + \Phi_2 \quad (8)$$

the velocity components are

$$v_r = v_{r_1} + v_{r_2} \quad (9)$$

und

$$v_\varphi = v_{\varphi_1} + v_{\varphi_2} \quad (10)$$

v_{r_1} is given by (4). At an outside point v_{r_2} is

$$v_{r_2} = \frac{\partial \Phi_2}{\partial r} = -f(t)\left[\frac{C_1}{(r/R)^2}\cos\varphi + \frac{C_2}{(r/R)^3}\cos 2\varphi + \ldots + \frac{C_9}{(r/R)^{10}}\cos 9\varphi\right]; \quad (11)$$

C_1, C_2 ... C_9 are the coefficients in (7). From (11) the additional potential follows at

$$\Phi_2 = \int v_{r_2}\, dr$$

$$= R\, f(t)\left[\frac{C_1}{r/R} \cos\varphi + \frac{1}{2} \frac{C_2}{(r/R)^2} \cos 2\varphi + \ldots + \frac{1}{9} \frac{C_9}{(r/R)^9} \cos 9\varphi \right] \qquad (12)$$

The total velocity v_r is

$$\frac{v_r}{a} = \cos\varphi \left[1 - \frac{1}{(r/R)^2} \right] - \frac{f(t)}{a} \left[\frac{C_1}{(r/R)^2} \cos\varphi + \frac{C_2}{(r/R)^3} \cos 2\varphi + \ldots + \frac{C_9}{(r/R)^{10}} \cos 9\varphi \right] \qquad (13)$$

and similarly

$$\frac{v_\varphi}{a} = -\sin\varphi \left[1 + \frac{1}{(r/R)^2} \right] - \frac{f(t)}{a} \left[\frac{C_1}{(r/R)^2} \sin\varphi + \frac{C_2}{(r/R)^3} \sin 2\varphi + \ldots + \frac{C_9}{(r/R)^{10}} \sin 9\varphi \right] \qquad (14)$$

from $$v_r = \frac{\partial\Phi}{\partial r} = \frac{1}{r} \frac{\partial\psi}{\partial\varphi}$$

and $$v_\varphi = \frac{1}{r} \frac{\partial\Phi}{\partial\varphi} = -\frac{\partial\psi}{\partial r}$$

the steam function follows at

$$\psi = -\int v_\varphi\, dr = r \int v_r\, d\varphi$$

$$= R\, a \sin\varphi \left[\frac{r}{R} - \frac{1}{r/R} \right] - R\, f(t) \left[\frac{C_1}{r/R} \sin\varphi + \frac{C_2}{(r/R)^2} \sin 2\varphi + \ldots + \frac{1}{9} \frac{C_9}{(r/R)^9} \sin 9\varphi \right] \qquad (15)$$

Now the question of pressure to be expected on the basis of our theorem is of particular importance.

Let p_1 be the pressure in the stagnation point at constant running speed of the cylinder and

$$w^2 = v_r^2 + v_\varphi^2$$

The pressure according to Bernouilli's equation is

$$p_1 = \rho \frac{w^2}{2} + p + \rho \frac{\partial \Phi}{\partial t}$$

p_1, the dynamic pressure, is sufficiently accurate at $1/2\rho a^2$. Herewith the pressure in dimensionless representation is

$$\frac{p}{1/2\rho a^2} = 1 - \frac{w^2}{a^2} - \frac{2}{a^2} \frac{\partial \Phi}{\partial t}$$

Inserting the computed values for v_r, v_φ and Φ the pressure equation then reads

$$\begin{aligned}\frac{p}{1/2\rho a^2} = 1 - \Bigg\{ & \Bigg\{ \cos\varphi \left[1 - \frac{1}{(r/R)^2} \right] - \frac{f(t)}{a} \left[\frac{C_1}{(r/R)^2} \cos\varphi \right. \\ & \left. + \frac{C_2}{(r/R)^3} \cos 2\varphi + \ldots + \frac{C_9}{(r/R)^{10}} \cos 9\varphi \right] \Bigg\}^2 \\ & + \Bigg\{ -\sin\varphi \left[1 + \frac{1}{(r/R)^2} \right] - \frac{f(t)}{a} \left[\frac{C_1}{(r/R)^2} \sin\varphi \right. \\ & \left. + \frac{C_2}{(r/R)^3} \sin 2\varphi + \ldots + \frac{C_9}{(r/R)^{10}} \sin 9\varphi \right] \Bigg\}^2 \\ & + \frac{2}{a} \frac{f'(t)}{a} R \left[\frac{C_1}{r/R} \cos\varphi + \frac{1}{2} \frac{C_2}{(r/R)^2} \cos 2\varphi \right. \\ & \left. + \ldots + \frac{1}{9} \frac{C_9}{(r/R)^9} \cos 9\varphi \right] \Bigg\} \end{aligned} \qquad (16)$$

With this our general considerations are terminated. However it should be emphasized that within the zone occupied by the vortices no correct result is afforded, as this zone is filled not by vortices but a potential flow. But this agrees outside of the vortices with the real flow only when the sources and sinks are correctly selected.

COMPARISON OF THEORETICAL AND EXPERIMENTAL DATA

1. Time function.- The $f(t)/a$ function must be so determined that the delimitation of the vortex zone (or the zero streamline) changes with the time in the same manner as observed in the test. The most characteristic point is the free stagnation point that moves on from the cylinder on the straight branch of the zero streamline. For it φ is always $\varphi = 0$, whereas the distance d from the center increases. In the free stagnation point both $v_\varphi = 0$ and $v_r = 0$. Hence with $r/R = d$

$$v_r = a\left(1 - \frac{1}{d^2}\right) - f(t)\left(\frac{C_1}{d^2} + \frac{C_2}{d^3} + \ldots + \frac{C_9}{d^{10}}\right) = 0$$

or

$$\frac{f(t)}{a} = \frac{1 - \frac{1}{d^2}}{\frac{C_1}{d^2} + \frac{C_2}{d^3} + \ldots + \frac{C_9}{d^{10}}}$$

Now $f(t)/a$ can be plotted against d; furthermore d can be plotted against the time t with the aid of the photographs. The position of the free stagnation point is indicated for the n^{th} picture at the moment $t_n = (n - 1)\,B + 1/2\,b_n$, where B, the total picture period = time of exposure + time necessary for transportation of the film and b_n is the time of exposure of the viewed picture. It is presumed thereby that the motion of the cylinder with respect to the water starts exactly with the exposure of the first picture.

Then the two curves enable the plotting of $f(t)/a$ against time t. From the second curve we take for a specific time t_b the related d and read off above its value on the first curve the respective value of $f(t)/a$,

which is then plotted against t_b and gives us the curve A of figure 14.

The term $\partial\Phi/\partial t$ in the pressure equation demands the derivation of $f(t)/a$ with respect to time. Graphical differentiation gives the curve B of figure 14. To facilitate the reading, we show $5f'(t)/a$.

The attempt of an approximate representation of the experimentally obtained curve for $f(t)/a$ by a e-function made an approximation of the form $f(t)/a = 0.135\ (e^{\beta t} - 1)$ seem appropriate, where $\beta = 1.295a/R$. In figure 14, A represents the experimental curve and C the approximation curve. A glance reveals that the rise of C in the range from $t = 0$ to $t = 7.5$ is greater than that of A, but smaller from $t = 7.5$ to about $t = 13.5$. For the prediction of the pressure $f(t)/a$ and $f'(t)/a$ are important factors, the widest departures of the approximated values from the experimental data, however, occur in a region where the vortex pair is not yet fully developed, that is, in a region of little interest.

2. Streamline pattern.- The streamlines are given by

$$\frac{\psi}{Ra} = \text{constant}$$

ψ/Ra is a function of φ and r/R which is written

$$\frac{\psi}{Ra} = G\left(\varphi, \frac{r}{R}\right)$$

The curves $G(\varphi, r/R)$, are computed by varying φ for a fixed r. They afford the basis for constructing the streamlines. The chosen example corresponds to picture 5 (fig. 5b) of our experiment. The result is illustrated in figure 15. The agreement with the test is very satisfactory.

3. Pressure on zero streamline.- Because our theorem does not represent the conditions in the vortex zone correctly, the calculation is limited to the pressure determination on the zero streamline. Hence equation (16) is to be numerically evaluated. Unfortunately it was found

that our method for predicting the pressure soon secured data which no longer take the experimental into account. For the earliest experimentally explored state with d = 1.17 and t = 6.7 the numerical calculation gives the curve A of figure 16; curve B of the figure is the experimentally obtained curve. Since the zero streamline in that state is not far from the body, curve C which indicates the pressure distribution for the usual potential flow at the cylinder circumference, was included for comparison; C' is the potential pressure curve corrected for scale effect.

In figure 17 the computed pressure curve for the same test at t = 10.05; d = 1.39 is shown as curve A, with the experimental curve B included for comparison. Our theorem actually suffices only for presenting the processes in the earliest stages with satisfactory approximation. As the development of the vortex pair progresses the pressures on the inflow side continue to rise faster according to the calculation, the pressure near the minimum is still fairly accurately represented; but then the flow-off side discloses large, continuously increasing deviations which, compared with the measured distribution show, first, pressure increase, then decrease. A greater number of terms in the series might perhaps afford a somewhat better agreement. The approach to the pressure in the free stagnation point is satisfactory again.

4. Field of pressure about the cylinder.- Figure 18 represents a computed picture of the pressure field for the state at t = 6.7 sec, d = 1.17 which does not agree very closely with the experimental picture in figure 7a on the flow-off side.

5. Pressure on the line of symmetry.- Plotting the pressures on the line $\varphi = 0$ against r/R for the flow picture 5a affords the curve A of figure 19. It shows behind the body that a point somewhat farther away from the cylinder rather than the free stagnation point corresponds to a pressure maximum. This corresponds with the experimental result in figure 8. A nonuniform stagnation point need not be a point of maximum pressure. The extent to which our simple theorem approaches reality is seen on the experimental curve B.

6. Pressure in the free stagnation point.- The pressure-drop in the free stagnation point is shown in figure 20. Curve A is theoretical, curve B experimental.

Both curves — the approximation of the calculation to the test is not unsatisfactory — first show a fairly rapid tendency toward a minimum below zero, then a gradual increase.

Translation by J. Vanier,
National Advisory Committee
for Aeronautics.

REFERENCES

1. Prandtl, L., and Tietjens, O.: Kinetographic Flow Pictures. T.M. No. 364, NACA, 1926.

2. Rubach, H.: Entstehung und Fortbewegung des Wirbelpaares hinter zylindrischen Körpern. Diss. Göttingen 1914.

3. Schmidt, F. S.: Zur beschleunigten Bewegung kugelförmiger Körper in widerstehenden Mitteln. Diss. Leipzig 1919.

4. Ermisch, H.: Abhandlungen aus dem Aerodynamischen Institut an der Technischen Hochschule Aachen, Heft 6. Julius Springer (Berlin), 1927.

5. Prandtl, L., and Tietjens, O.: Hydro- und Aeromechanik, Bd. I, p. 154 (Berlin), 1929.

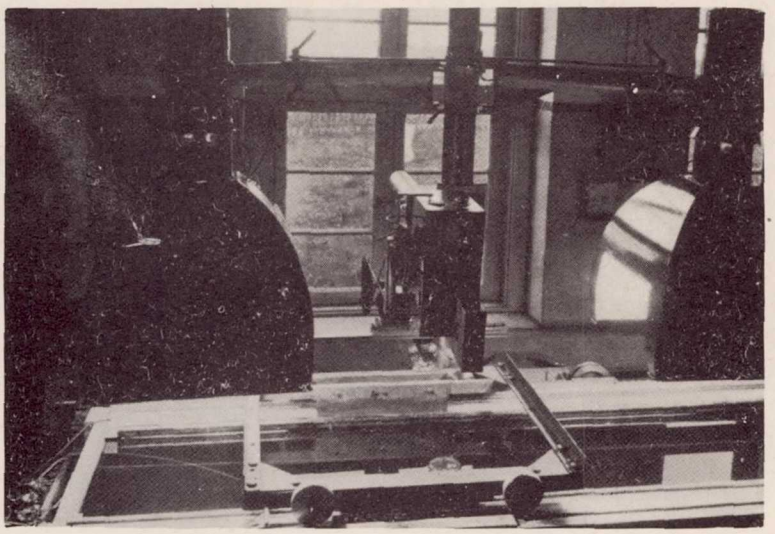

Figure 1.- View of experimental set-up.

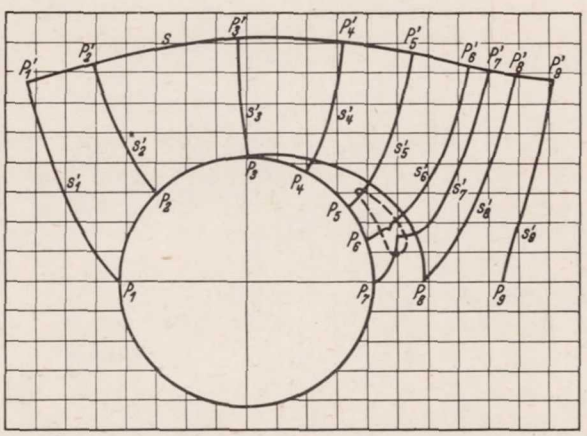

Figure 2.- Streamline and vertical lines secured from fig. 5b.

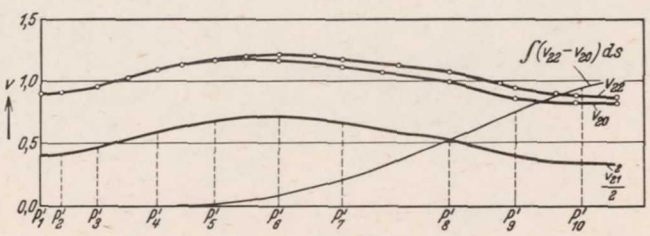

Figure 3.- Velocities plotted across the extended streamline. Streamline s is not that of fig. 2, but taken from a later state (fig. 5e) for reasons of clarity.

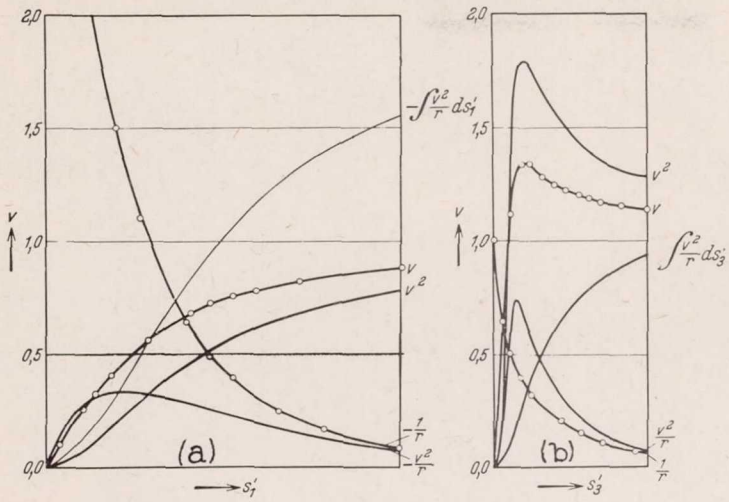

Figure 4.- Velocity and curvature plotted against the extended vertical lines; s'_1 and s'_3 taken from fig. 2.

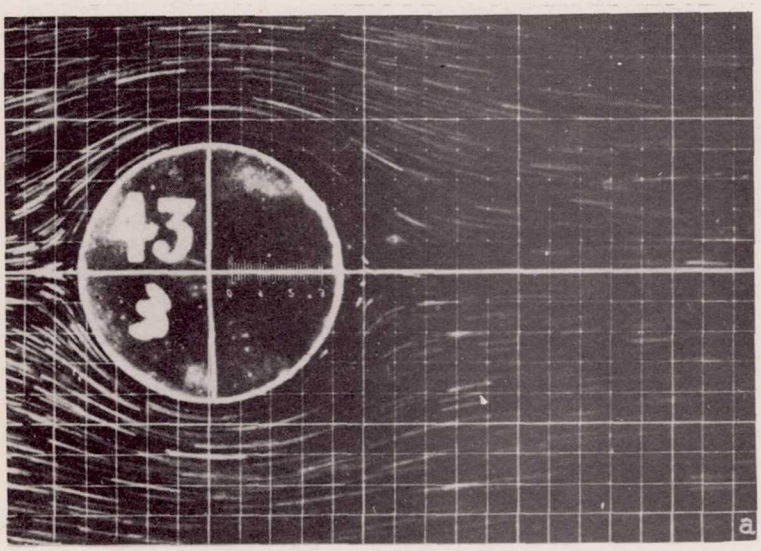

Figure 5(a to e).- Evaluated development stages of the starting vortex pair. The running speed of the cylinder is a = 0.82 cm/s, the diameter is 2R = 8.5 cm. At a kinematic viscosity of water of $\nu = 0.0125$ cm^2/sec. The Reynolds number is Re = a2R/ν = 560.

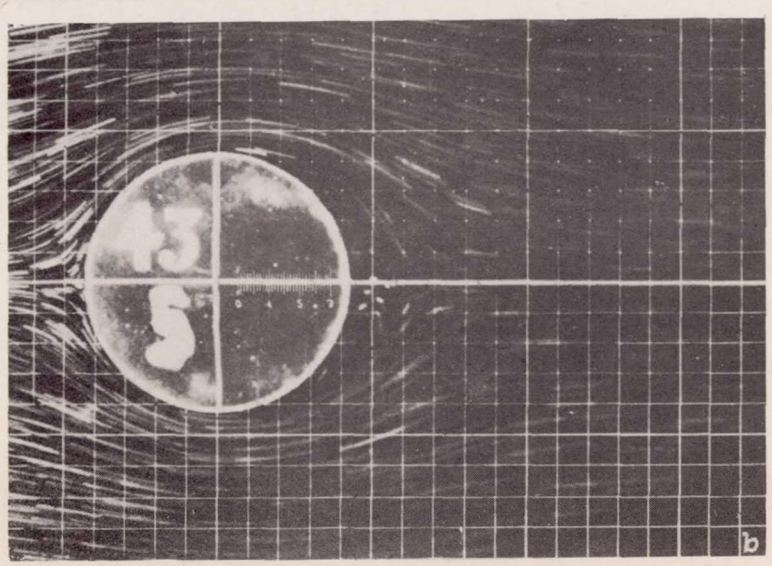

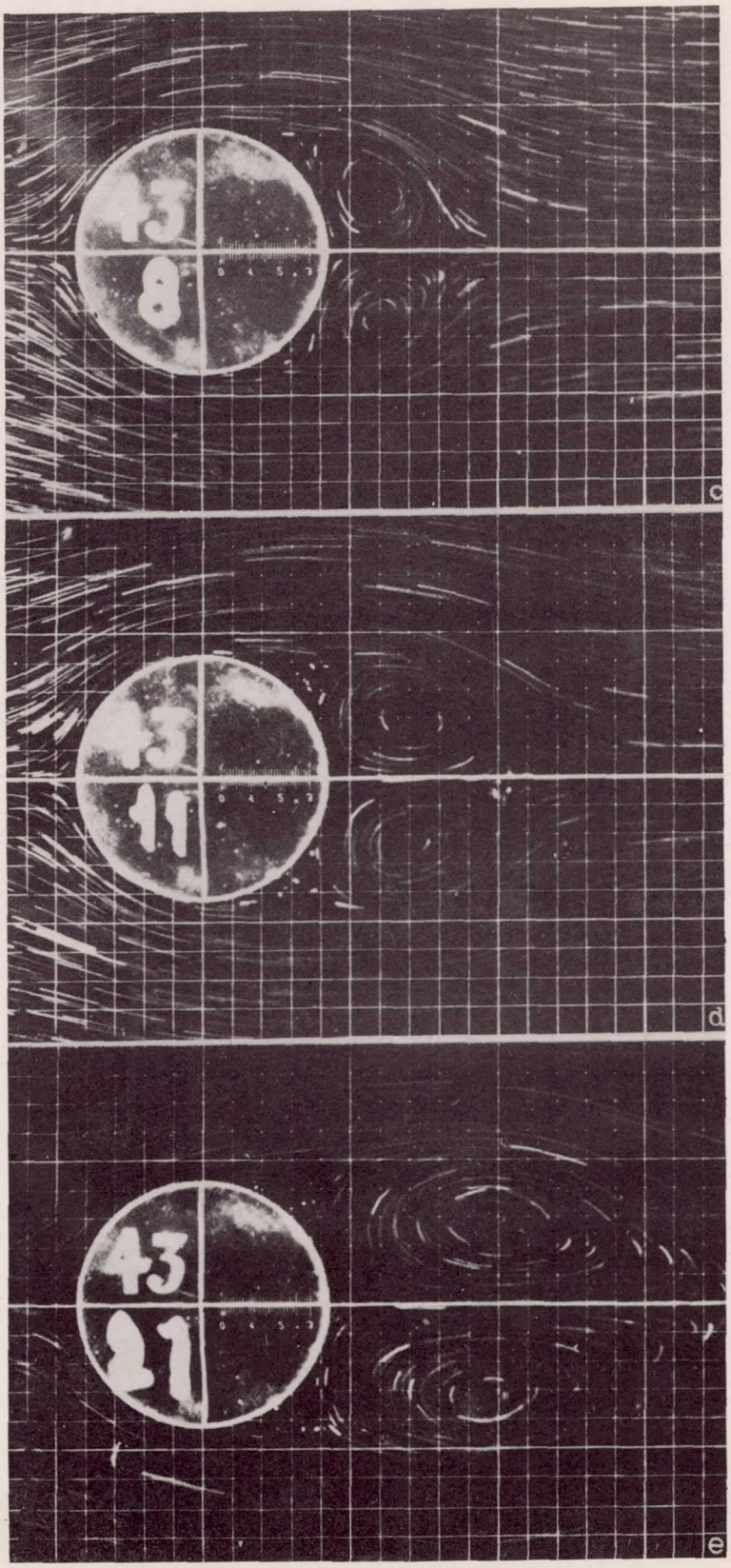

Figure 5.- Concluded.

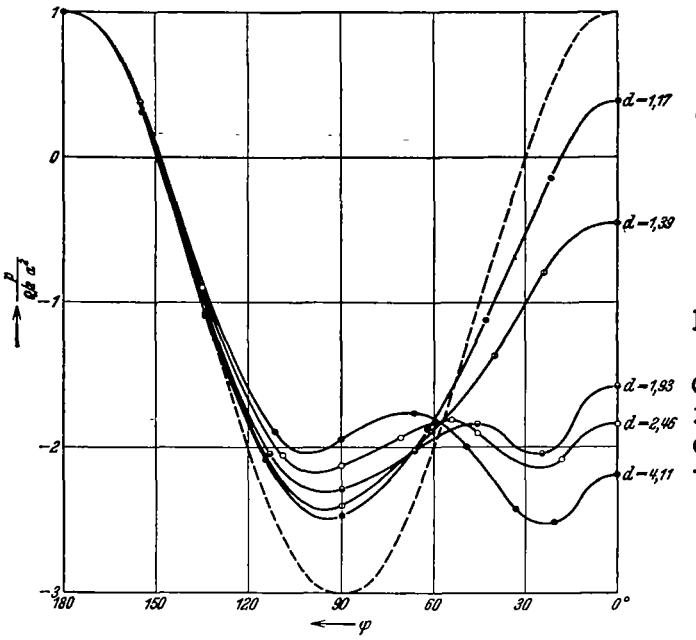

Figure 6.- Pressure distribution over half the cylinder circumference for the development stages of the vortex pair shown in fig. 5a to 5e.

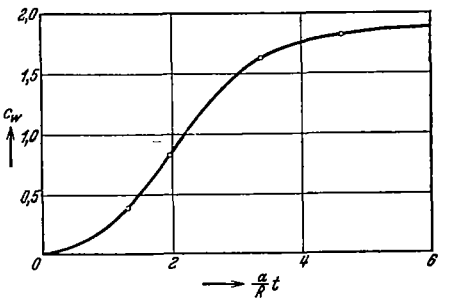

Figure 9.- Time rate of change of drag coefficient of cylinder during the growth of the vortex pair, (at $ta/R = 9$, $c_w = 2.07$).

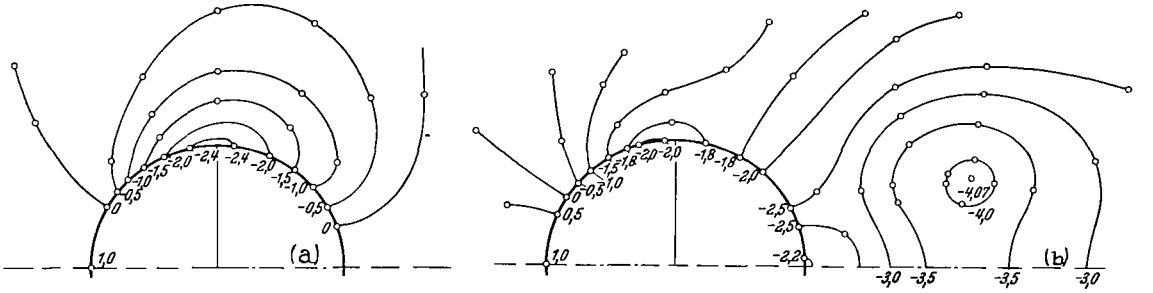

Figure 7.- Lines of equal pressure, a according to fig. 5a, b according to fig. 5e.

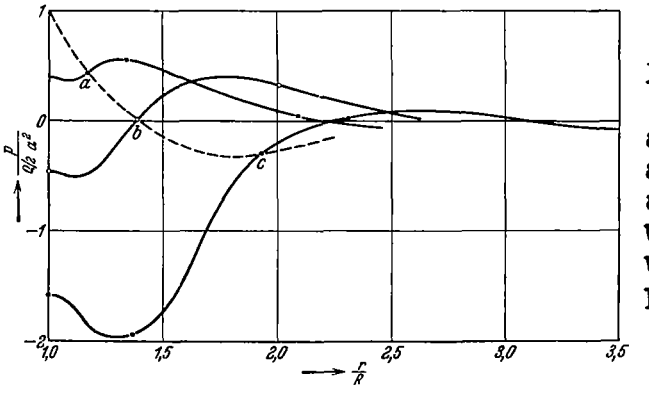

Figure 8.- Pressure on the symmetry line, a according to fig. 5a, b according to fig. 5b, c according to fig. 5c, to which is added a point with $r/R = 3.9$. $p/1/2\rho a^2 = -0.112$.

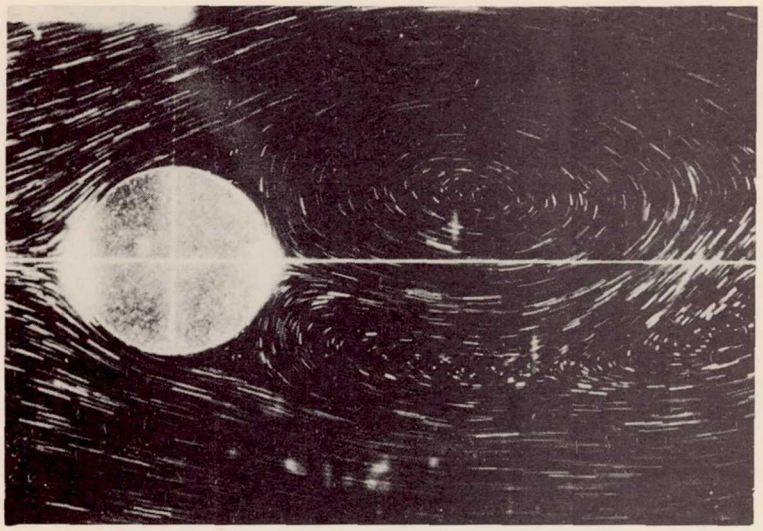

Figure 10.- A symmetrical vortex arrangement in the vortex sheet, Re = 735.

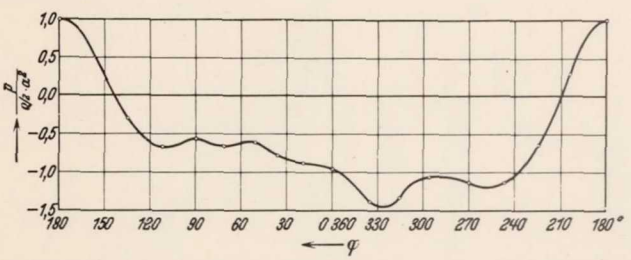

Figure 11.- Pressure distribution over the cylinder circumference according to fig. 10.

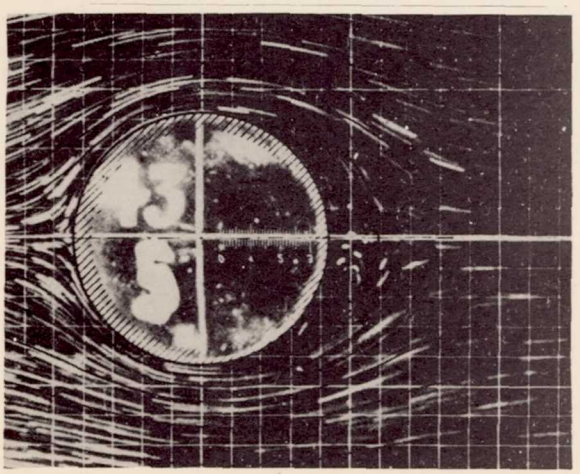

Figure 15.- Theoretical streamline picture transferred to the corresponding record.

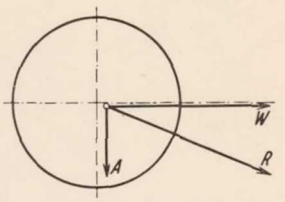

Figure 12.- Drag and transverse force on the cylinder according to fig. 10; the resultant passes through the center.

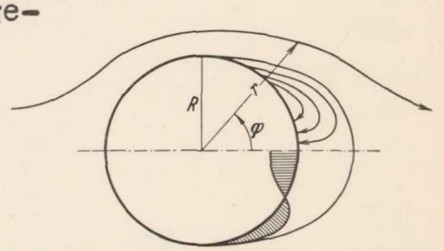

Figure 13.- Explanatory figure, top: replacement of vortex zone within the zero streamline by a source-sink flow, bottom: illustration of rule of formation.

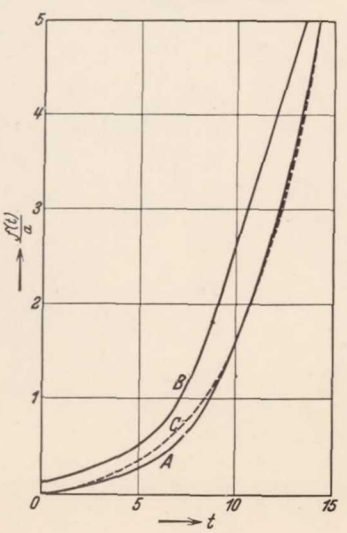

Figure 14.- Aspect of time variable f(t)/a (curve A), its derivation (curve B, here 5f'(t)/a), and approximation by an e function (curve C).

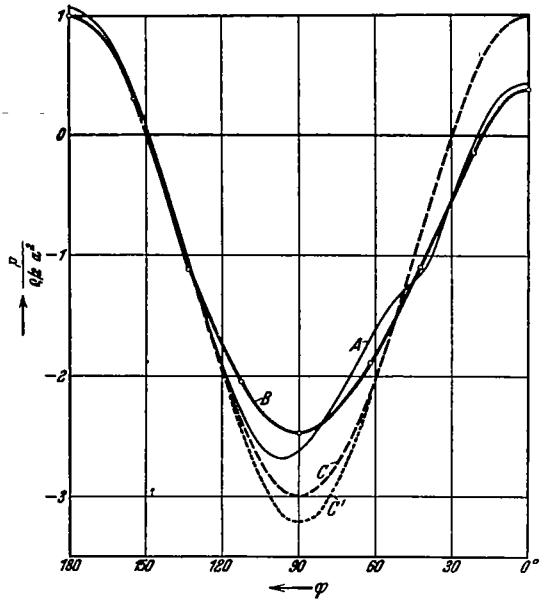

Figure 16.- Pressure distribution on zero streamline according to fig. 5a. A is computed, B experimental curve, C potential pressure curve at cylinder, C' the same corrected for scale effect.

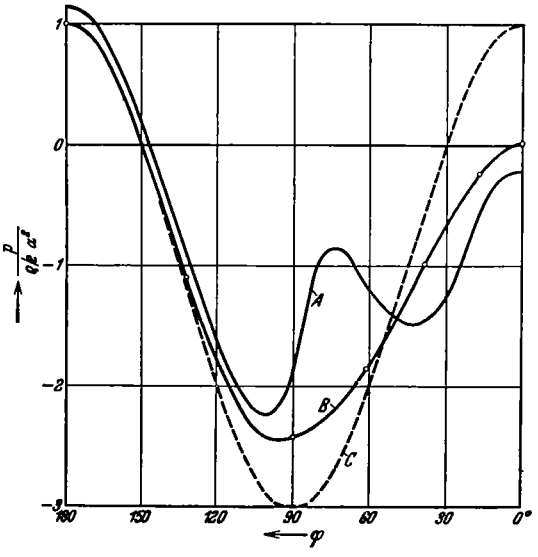

Figure 17.- Pressure distribution on zero streamline according to fig. 5b; A theoretical, B experimental curve.

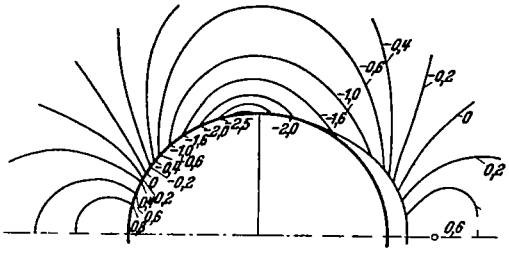

Figure 18.- Theoretical pressure according to fig. 5a, the experimental result is shown in fig. 7a.

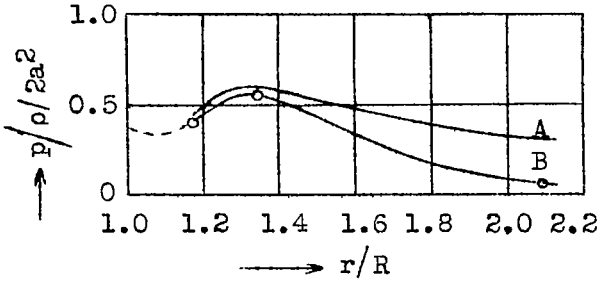

Figure 19.- Pressure on the symmetry line outside of the free stagnation point according to fig. 5a; A theoretical, B experimental curve.

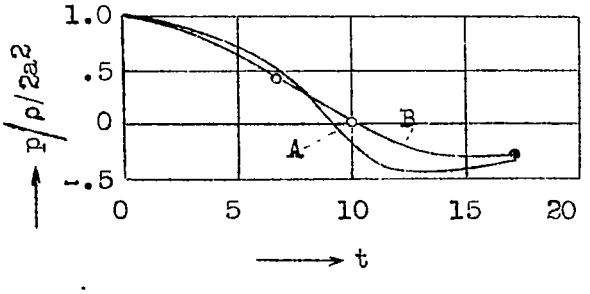

Figure 20.- Time rate of change of pressure in free stagnation point; A theoretical, B experimental curve.